Report
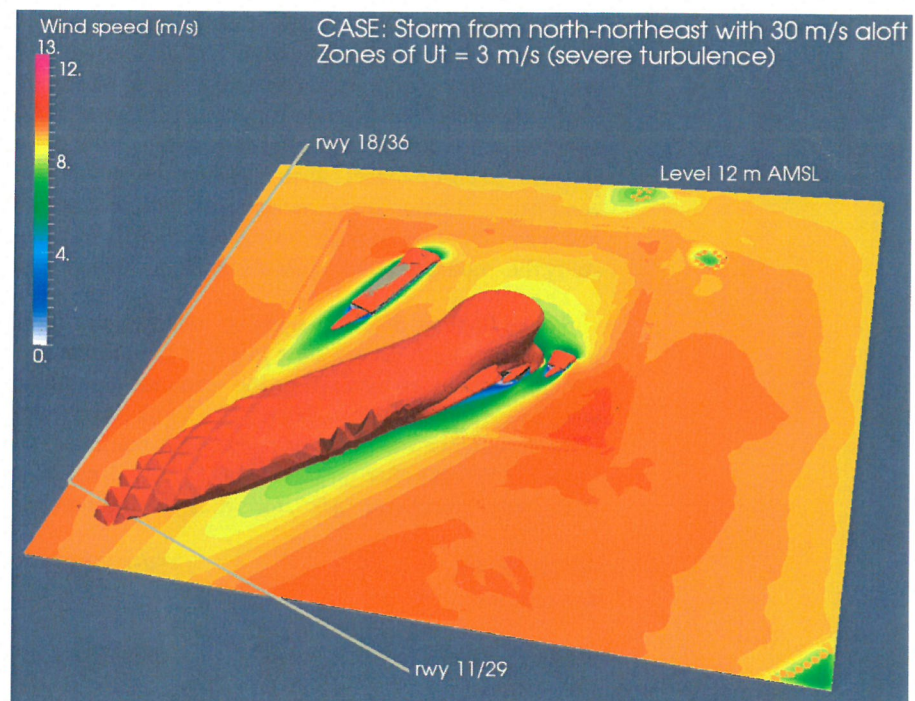
Analysis of Turbulent Wakes Behind Helicopter Hangars at Sola Airport

Author(s)
Karstein Sørli   Mandar Tabib   Adil Rasheed

Air volumes (illustrated by orange iso-surfaces) of *severe turbulence* caused by storm from north-northeast perpendicular to the new and planned helicopter hangar at Stavanger Airport Sola. Wind speed aloft 30 m/s and idealized vertical wind profiles at inflow boundaries.

Report

Analysis of Turbulent Wakes Behind Helicopter Hangars at Sola Airport

VERSION	**DATE**
2.0	30th June 2015

AUTHOR(S)
Karstein Sørli   Mandar Tabib   Adil Rasheed

ABSTRACT
Turbulence in the wake generated by airflow over buildings may produce complex airflow patterns in the downwind region. Examples include the recirculating flow and wind deficit areas behind airport buildings and their potential impact on flight conditions at runways. In this study a computational fluid dynamics analysis of the airflow over helicopter hangars was performed, including the turbulent wakes that were generated behind the hangars. The effects of the wakes on landing and departing aircraft on the two runways (18/36 and 11/29) at Sola were estimated, based on a number of numerical simulations. With the prevailing wind direction at Sola, the airport hangars cause no effects on aircraft landing and taking off. Strong wind perpendicular to the hangars, is a different scenario and is the most critical one when it comes to wake turbulence. Simulations were therefore performed to study the impact of building wakes under such conditions.

The main findings of the analysis are that *aviation turbulence* at free wind speeds of 20 m/s for both runways are just light to moderate at delimited runway sections behind the hangars for each of the scenarios mentioned. However, when the free wind speed increases from 20 m/s to 30 m/s (from fresh gale to violent storm), the wake turbulence may be severe for both scenarios. However, the unfavourable impact of the NEW hangar on runway 11/29 will not be as large as the impact of the OLD hangar on runway 18/36, for similar wind conditions.

SINTEF

Document History

VERSION	DATE	VERSION DESCRIPTION
version	date	description
1	11th June 2015	Preliminary version with a summary and the conclusions in Norwegian
2	26th June 2015	pre-Final unsigned version
3	30th June 2015	Final version

PROJECT
102011078

REPORT NUMBER
SINTEF A27088

VERSION
3.0

2 of 27

SINTEF

Contents

ATTACHMENTS

Nomenclature

AMSL	Above Mean Sea Level
CFD	Computational Fluid Dynamics
RWY	runway
UTM	Universal Transverse Mercator

Oppsummering og konklusjoner på norsk

Hovedmålet med denne analysen har vært å finne ut om en planlagt oppføring av ny helikopterhangar ved Stavanger lufthavn Sola vil kunne ha en uheldig innvirkning på flyforholdene over og i nærheten av de to rulle-banene ved denne flyplassen. Selv om den gamle helikopterhangaren skal rives om en stund ble det besluttet også å studere virkningene av denne, spesielt med henblikk på et mulig uheldig samvirke mellom de to hangarene i den tiden begge står der. Med uheldige virkninger i denne sammenheng menes i første rekke *turbulente vaker* som ofte genereres av hangarene under gitte vær- og vindforhold og som kan strekke seg helt bort til en av rullebanene. Det er tidligere etablert grenseverdier for *svak turbulens*, *moderat turbulens*, *alvorlig turbulens* og *ekstrem turbulens* basert på en størrelse kalt *turbulensintensitet* (U_t), som er definert som kvadratroten av *turbulent kinetisk energi* ($\sqrt{k}$) i luftstrømmen (som gir enheten m/s). Selv om endringer i vindstyrke og vindretning (vindskjær) ofte medfører turbulens, er det nyttig å studere vindfeltene direkte over rullebanene med henblikk på risikoen for tap av *aerodynamisk løft* som eksisterer i kritiske øyeblikk av en landing eller avgang. Imidlertid er det viktig å presisere at våre analyserer baserer seg hovedsaklig på turbulensintensiteten som beregnes med våre matematiske modeller. Dette er en godt utprøvd og validert metodikk som er anvendt flere ganger tidligere.

Måten vi har utført denne analysen på er gjennom *numeriske simuleringer av vindfelt og turbulens*, basert på matematiske ligninger som beskriver tre-dimensjonal luftstrømning og som løses ved hjelp av en datamaskin. Dette er meget beregningskrevende ligninger og modeller som selv med en kraftig, parallell-prosesserende datamaskin må kjøres i mange timer. Til sammenligning med de operative modellene som kjøres for vars-ling av *terrengbasert turbulens* ved 20 norske flyplasser i dag (samarbeid mellom Meteorologisk institutt og SINTEF), så er simulering av *bygningsbasert turbulens* en mye mer krevende oppgave begningsteknisk sett, selv om det i prinsipp er de samme ligningene som løses. Hovedgrunnen til dette er forskjellen i krav til romlig oppløsning. For bygningsbasert turbulens er dette oppløsningskravet to ordener større (anslagsvis 1 m versus 100 m horisontalt).

Det aktuelle området som ble analysert er $750 \times 750 \times 500$ m stort (500 m vertikalt) med hangarbygningene i senter av dette området. Størrelsen på bygningene ble lest ut fra tegninger tilsendt fra oppdragsgiver, mens deres beliggenhet i det aktuelle terrenget ble estimert ved å legge en detaljtegning av bygninger og veier rundt hangarene inn i *Google Earth* og lese UTM-koordinatene derfra. Deretter ble bygningene og terrenget triangulert og videreført til en program for diskretisering (meshing) av det aktuelle området på flyplassen. Dette er også en tidkrevende prosess som krever kvalitetssjekking av meshet. Kvaliteten er helt avgjørende for at simuleringene skal gå raskest mulig og for at resultatene (bl.a. vindfelt og turbulensintensitet) skal bli mest mulig nøyaktig.

Deretter ble et 3D fluiddynamisk simuleringsprogram benyttet. Tre forskjellige vindretninger ble simulert, $25°$ (nord-nordøstlig (N-NØ)), $115°$ (øst-sørøstlig (Ø-SØ)) og $270°$ (vestlig (V)). Den siste vindretningen (V) ble simulert fordi det er den mest vanlige vindretningen på dette stedet. Den var imidlertid ikke ventet å gi noen negative effekter fra hangarene for flytrafikken på hverken den ene eller den andre rullebanen. Simuleringene som ble utført bekreftet også det. De to første vindretningene (N-NØ og Ø-SØ) ble valgt ut for å frembringe de mest uønskede forholdene over de to rullebanene, forårsaket av vind vinkelrett inn mot h.h.v. den nye og den gamle hangaren. Dette genererer en turbulent vake mellom hangaren og rullebanen. Hovedspørsmålet var om denne sonen ville strekke seg hele vegen fra hangaren til rullebanen og kanskje over denne, og være så sterk at den kunne innvirke på fly som lander og tar av her. Som nevnt ovenfor har vi sett på både hvordan vinden endrer seg og hvordan turbulensintensiteten over rullebanen blir med de gitte vindretningene. Høydevinden som har blitt benyttet i alle tre tilfellene har vært 20 m/s og et idealisert, vertikalt vindprofil ble brukt som innstrømsbetingelse til den 3-dimensjonale modellen. I tillegg er en gitt turbulensintensitet på innstrømsflatene antatt.

Følgende konklusjoner er foretatt etter at simuleringene var gjennomført og resultatene var visualisert (se et utvalg av plottene i figurene 7, 8) og analysert:

1. Vestlig vindretning ($270°$) (den oftest forekommende) skaper ingen problemer isolert sett fra ny og gam-mel hangar, siden de turbulente vakene fra både den nye og den gamle hangaren i dette tilfellet ligger langt unna rullebanene. Det bør nevnes at terminalbygget som ligger på oppvindsiden av rullebane 18/36 ikke var med i dette simuleringsoppsettet. Vår oppgave i denne omgang var å studere effektene fra ny og

gammel hangar isolert sett og i gjensidig samspill, men ikke i samspill med andre bygninger på flyplassen som f.eks. terminalbygget.

2. Nord-nordøstlig (N-NØ, $25°$) vindretning skaper forhold som ligger i grenseland med hensyn til uønskede effekter fra den nye hangaren. Dette er en vindretning som sammen med den nye hangaren lager den lengste og kraftigste turbulente vaken i retning bane 29. Vindfeltet kan skape vindskjær ved denne banen. Turbulensintensiteten er svak til moderat over banen, vel og merke med 20 m/s (sterk kuling til liten storm) høydevind 1500 m AMSL. Siden *nøytral atmosfære* er antatt for disse simuleringene, kan våre simuleringsresultater skaleres lineært med økende høydevind. Vindmålinger på Sola har flere ganger vist hastigheter opp mot 30 m/s (sterk storm) for midlere vind. Det betyr at vi kan multiplisere turbulens-intensiteten med en faktor 1.5 i dette tilfellet. Da beveger vi oss fra $U_t = 2$ til $U_t = 3$ over rullebanen og vi har gått fra svak/moderat turbulens til moderat/alvorlig turbulens. Konklusjonen er derfor at den nye hangaren medfører akseptable flyforhold (svak til moderat turbulens) ved rullebane 29 ved N-NØ-lig vindretning og vindstyrke opp mot 20 m/s i høyden, mens sterk storm (30 m/s) kan gi alvorlig turbulens over banen forårsaket av den nye hangaren.

3. Øst-sørøstlig (Ø-SØ, $115°$) vindretning skaper forhold som ligger i grenseland med hensyn til uønskede effekter fra den gamle hangaren. Dette er en vindretning som sammen med den gamle hangaren lager den lengste og kraftigste turbulente vaken i retning bane 18/36. Vindfeltet kan skape vindskjær ved denne banen. Turbulensintensiteten er svak til moderat over rullebanen, men på samme måte som for det forrige scenariet (N-NØ vind) endrer bildet seg ved å øke høydevinden fra 20 m/s til 30 m/s (fra sterk kuling til sterk storm). Forholdene er faktisk en tanke verre her enn for den nye hangaren og N-NØ-lig vind. Konklusjonen er derfor at den gamle hangaren medfører akseptable flyforhold (svak til moderat turbulens) ved rullebane 18/36 ved S-SØ-lig vindretning og vindstyrke opp mot 20 m/s i høyden, mens sterk storm (30 m/s) kan gi alvorlig turbulens over banen forårsaket av den gamle hangaren.

4. Vi fant intet uheldig samvirke av ny og gammel hangar gjennom de simuleringene som ble utført. Her lå det i utgangspunktet en mulighet for et slikt samvirke ved Ø-SØ-lig vindretning, men simuleringen viser kun en minimal effekt i den retning. Konklusjonen er derfor at det ikke ville kunne inntre ugunstige flyforhold ved bane 18/36 som følge av samvirke mellom ny og gammel hangar i den tiden begge står oppført.

5. Et annet poeng som bør nevnes er at den nye (planlagte) hangaren er mindre ugunstig m.h.t. turbulente vaker enn den gamle når de sammenlignes med hver sin mest ugunstigste vindretning, henholdsvis N-NØ og S-SØ.

Den nye hangaren kan m.a.o. komme til å forverre flyforholdene på bane 29, men dens ugunstige påvirkning vil ikke bli så stor som den gamle hangarens påvirkning på flyforholdene for bane 18/36.

PROJECT
102011078
REPORT NUMBER
SINTEF A27048
VERSION
2.0
7 of 27

1   Introduction

Air recirculations and wakes due to wind flow over buildings may induce a variety of uncertainties in the down-wind area of the buildings. Wind tunnel and water channel experiments have often been employed to investigate the aerodynamic effects of the wake behind buildings and have been used to complement field measurements. However, they are costly and time-consuming to conduct with high accuracy. With the increasing computational power-to-cost ratio of modern computers, computational fluid dynamics (CFD) techniques are now affordable alternatives for examining the impact of buildings on downwind areas like runways of an airport.

Owing to the cost-effectiveness of CFD, numerous investigations have been performed to study wind behavior in the wake behind buildings. Senthooran et al. (2004) used CFD to study the flow-induced pressure fluctuation around a low-rise building. Huang et al. (2007), using different CFD turbulence models, compared the mean and dynamic wind load on tall buildings. Apart from wind load calculations, Krüs et al. (2003) used CFD to determine the effects of isolated roughness elements and an industrial complex on the wind environment of an adjacent airfield. Neofytou et al. (2006) focused on the turbulence generated by an obstacle on a wind field and the in-flight conditions over the nearby runway. The objective of the studies by Krüs et al. (2003) and Neofytou et al. (2006) was to assess the reliability of CFD for the investigation of wind behavior at airports by comparing modeling results and field measurements. Generally, they arrived at a common conclusion that the wake behind a building posed a significant threat to aircraft over a nearby runway. Thus, certain safety criteria and precautionary measures have been recommended for safe aviation operation. These studies considered only rather limited ranges in the background wind speed and direction.

In this study, a number of CFD simulations were performed of wind flow around a small cluster of airport buildings consisting of two hangars and two smaller buildings. One of the hangars was already there, while the other hangar and the other two smaller buildings were on the planning stage. The main purpose of the study was to investigate the potential impact of the new buildings on the flight conditions at the airport. The analysis was performed by considering various background wind speeds and directions with respect to the buildings. We investigated the effects of building wakes and recirculations and their potential impact on landing and departing aircraft on two nearby runways.

2   Method

This section gives a theoretical foundation of the analysis presented in the following sections.

2.1   Governing Equations

A transient 3D CFD model incorporating complex terrain, building features and turbulence modeling is developed. The model computes velocity, pressure, temperature and the turbulence fields arising out of an interaction between the flow and the terrain and buildings. The turbulence in this case is modeled using a RANS (Reynolds Averaged Navier Stokes) approach. The equations for the RANS model (Equations 1-3) have been derived by applying the Reynolds averaging to the Navier-Stokes equations. $\mathbf{u}, p, \theta, \rho$ in the equations represent time averaged velocity, pressure, potential temperature and density respectively. The three equations below represent the conservation of mass (Equation 1), momentum (Equation 2) and energy (Equation 3). For neutral conditions, the energy equation is omitted.

$$\nabla \cdot (\rho_s \mathbf{u}) = 0 \tag{1}$$

$$\frac{D\mathbf{u}}{Dt} = -\nabla \left(\frac{p_d}{\rho_s} \right) + \mathbf{g}\frac{\theta_d}{\theta_s} + \frac{1}{\rho_s}\nabla \cdot \mathbf{R} + \mathbf{f} \tag{2}$$

$$\frac{D\theta}{Dt} = \nabla \cdot (\gamma_T \nabla \theta) + q \tag{3}$$

The term $R_{ij} = \nu_T \left(\frac{\partial u_i}{\partial x_j} + \frac{\partial u_j}{\partial x_i} \right) - \frac{2}{3} k \delta_{ij}$ in Equation 2 arises from the averaging procedure and is referred to as turbulent stresses. $\mathbf{f}$ is a source term that may include rotational effects of the earth, $\mathbf{g}$ is the gravitational acceleration, γ is the thermal diffusivity and q is the energy source term. Subscript s indicates hydrostatic values and subscript d the deviation between the actual value and its hydrostatic part, i.e. $p = p_s + p_d$, $\theta = \theta_s + \theta_d$, $\rho = \rho_s + \rho_d$, where the hydrostatic part is given by $\partial p_s / \partial z = -g\rho_s$. In addition, the following expression for hydrostatic density may be derived from the state equation and the definition of potential temperature:

$$\rho_s = \frac{p_s}{R_o \theta_s} \left(\frac{p_o}{p_s} \right)^{R/C_p} \tag{4}$$

where R_o is the gas constant and C_p is the specific heat at constant pressure. Hence, once the hydrostatic (potential) temperature profile is given, the hydrostatic pressure and density may be calculated, and then substituted into Equations 1 and 2.

It may be noted that the Boussinesq approximation is obtained from the system of Equations 1 and 2 by assuming constant values (ρ_o, θ_o) instead of the hydrostatic values, and that formulation may well be used for incompressible flow and ordinary temperature. Computation of eddy viscosity $\nu_t = \mu_t / \rho_s$ is needed for the closure of the Equation set (1-3). This quantity is dependent on the turbulence model (as described below). When $k - \epsilon$ model is used, the turbulent eddy viscosity is formulated in terms of turbulent kinetic energy (k) and eddy dissipation rate. These two are obtained by solving their transport equations as in Equation 6 and 7.

$$\mu_t = C_\mu \frac{k^2}{\epsilon} \tag{5}$$

$$\frac{DK}{Dt} = \nabla \cdot (\nu_T \nabla K) + P_k + G_\theta - \epsilon \tag{6}$$

$$\frac{D\epsilon}{Dt} = \nabla \cdot \left(\frac{\nu_T}{\sigma_e} \nabla \epsilon \right) + (C_1 P_k + C_3 G_\theta) \frac{\epsilon}{k} - C_2 \frac{\epsilon^2}{k} \tag{7}$$

where P_k and G_θ are production of turbulent kinetic energy due to shear and buoyancy and are described below :

$$P_k = \nu_T \left(\frac{\partial u_i}{\partial x_j} + \frac{\partial u_j}{\partial x_i} \right) \frac{\partial u_i}{\partial x_j}, \quad G_\theta = -\frac{g}{\theta} \frac{\nu_T}{\sigma_T} \frac{\partial \theta}{\partial z} \tag{8}$$

2.2 Solver details

The solver has been created in OpenFOAM-2.3.0 (OF). To ensure continuity, i.e. conservation of mass, an elliptic equation for the modified pressure is created by combining the continuity equation with divergence of momentum equation. This elliptic equation along with the momentum equation, energy equation and turbulence equations are solved in a segregated manner using the PISO-SIMPLE (PIMPLE) algorithm (a hybrid of the SIMPLE and PISO algorithms). The PIMPLE algorithm allows use of a larger time-step for transient simulations. The OF uses a finite volume discretization technique, wherein all the equations are integrated over control volumes (CV) using Green Gauss divergence theorem. The Gauss divergence theorem converts the "volume integral of divergence of a variable" into "surface integral of the variable over faces comprising the CV". Thus, the divergence term defining the convection terms can simply be computed using the face values of variable in the CV. The face values of variable are obtained from its neighboring cell centered values by using convective scheme. In this work, all the equations (except k and ϵ) use second order linear discretization scheme, while the turbulent equations use upwind convection schemes. Similarly, the diffusion term involving laplacian operator (the divergence of the gradient) is simplified to computing the gradient of the variable at the face. The gradient term can be split into contribution from the orthogonal part and the non-orthogonal part. A full non-orthogonal correction is implemented for all equations as solver stability won't be a problem owing to good mesh used. The mesh details, CFD domain set-up, boundary and initial conditions are defined below.

2.3 Safety Analysis

The simplest meteorological variable considered most important for aviation safety is called the $F-$factor or wind shear and what is called turbulence, represented by $\epsilon^{1/3}$. These quantities are given by Equations 9 and 10

$$F = -\overline{\frac{c}{g}\frac{\partial u}{\partial x} + \frac{w}{c}}^{\ell_f} = -\frac{c}{g\ell_f}[u(x+\ell_f/2) - u(x-\ell_f/2)] + \frac{\overline{w}^{\ell_f}}{c} \tag{9}$$

$$\epsilon^{1/3} \approx \left(\frac{(C_\mu^{1/2}K)^{3/2}}{\ell_t}\right)^{1/3} \approx 0.67K^{1/2}\ell_t^{-1/3} \tag{10}$$

Here c is the fly path, g is the acceleration due to gravity, u is the wind component along the fly path, w is the vertical wind component, ϵ is the turbulent dissipation, K is turbulent kinetic energy, ℓ_t turbulent length scale and ℓ_f is the minimum response distance for landing configuration and is of the order of $\sim 500\,m$, which corresponds to a time interval of about $t = O(7\,s)$. Averaging over this distance is indicated by the overline. Coefficient C_μ is given by $C_\mu \approx 0.09$. A good review of this theory can be found in the paper by Eidsvik et al. (2004).

Prevalence of the two conditions $F < -0.1$ and $\epsilon^{1/3} > 0.5\,m^{2/3}s^{-1}$ correspond to severe turbulence for commercial aircraft and represent potential danger (Clark et al. (1997)). These conditions are easily met when $\sqrt{K} > 3$. This quantity is called *turbulence velocity* (U_t) and has unity m/s. Thresholds for *light turbulence*, *moderate turbulence*, *severe turbulence* and *extreme turbulence* have been established in the past, based on the value of $U_t = \sqrt{K}$.

3 Simulation Set-up

3.1 Domain size and mesh

The dimensions of the buildings were extracted from the illustrations that the client sent us. Their exact locations were estimated by taking a detailed image of buildings and roads around the hangars and importing it in *Google Earth* as a so-called *overlay image*, and thereafter reading the UTM coordinates of the building corners. This is illustrated in Figure 1 of Appendix A. All corner coordinates were extracted in this way. However, it is possible to do this a bit simpler and even more exact by using the UTM coordinates of just one corner of a building and the angle between the west-east axis and one side of the building. Knowing the length of all sides of the building, given a rectangular building, all other building corner coordinates can easily be determined. In case of a building with sections of different heights, the procedure has to be repeated for each section. In the present study all buildings or sections were assumed to have a flat roof.

The actual airport area that was analysed is $750 \times 750 \times 500$ m large (500 m vertically) with the hangar buildings approximately in the center of this domain. In Figures 2 and 4 (zoomed in) of Appendix A this setup is illustrated with both the old and the new hangar as well as part of the centerline of the two runways. A digital elevation map of the airport region was generated from the terrain data available with Norwegian Mapping Authority (http://www.norgeskart.no). Finally, the buildings and terrain within the chosen area were triangulated and given as input to a software tool for the volume discretization (meshing) of the whole domain of investigation at the airport. This is also a time consuming process which needs a through mesh quality check. The mesh quality is important to facilitate fast simulations as well as to get results (e.g. wind field and turbulence) that are as accurate as possible. This domain was spatially discretized such that the maximum grid size was $50m$, while the mesh in regions near the terrain and building were highly refined (approximately $1m$). This finer mesh resolution enabled us to capture the shear and subsequent turbulence generation in wind due to obstruction from terrain features and the building. The mesh has passed all quality parameter checks and the mesh size is fine enough to yield high quality results. In Figure 3 of Appendix A this is shown with several intersecting mesh planes with the new hangar in focus. In Figure 6 of Appendix A is shown a terrain map around the hangars. The variation is only a few meters so there should be no significant interaction between the terrain

and the buildings. What could be significant is the interaction with other buildings that are located near to the hangars on their upwind sides. This is not analyzed in the present study.

3.2 Weather conditions as input boundary conditions for simulations

In complicated mountainous terrain it is generally difficult to specify a realistic inlet profile. Therefore, a standard profile for wind speed and turbulent kinetic energy was used to specify the boundary conditions and initialize the domain. The profiles for the wind speed $u_0(z)$ and the turbulent kinetic energy $K_0(z)$ are given by

$$u_0(z) = \frac{u_*}{\kappa} \left(ln\frac{z}{z_0} + W(\frac{z}{D}) \right) \tag{11}$$

$$K(z) = C_\mu^{-1/2} u_*^2 \left(1 - \frac{z}{D} \right) \tag{12}$$

$$\epsilon(z) = \frac{C_\mu^{3/4} K(z)^{3/2}}{\kappa z} \tag{13}$$

where u_*, z_0, z and D represent friction velocity, surface roughness, height above the ground surface and boundary layer thickness, respectively. The so-called wake function W is defined by the formula $W(z/D) = (A - 1)(z/D) - A/2(z/D)^2$ such that $W(1) = 1$. The coefficients $\kappa = 0.42$ and $A = 4.0$. Synoptic wind (mesoscale) U is given by $U = u_0(D)$. In the present simulations we have used $(z_0, D, U) = (0.3\,m, 1500\,m, 20\,m/s)$. This means that the maximum wind speed of $20\,m/s$ is obtained at height of $1500\,m$ above sea-level. Three different wind directions were simulated, i.e. 25° (north-northeasterly (N-NE)) (illustrated in Figure 5 of Appendix A), 115° (east-southeasterly (E-SE)) and 270° (westerly (W)) were simulated. The last wind direction (W) was added because this is the prevalent wind direction at the given site.

3.3 Hardware configuration

Each run was conducted on 16 processors, with each processor of make Intel(R) Xeon(R) CPU E5-2650 0 @ 2.00GHz. The steady state simulation for each run took around one day.

4 Discussion of Simulation Results

Figure 7 of Appendix B shows the contours of wind speed and turbulence velocity at four different heights (22m, 18m, 14m and 10m) for the N-NE-erly wind direction. It is very clear from the figure that the velocity deficit and wakes induced by the buildings can reach and intersect one end of runway 11/29. The effect is most pronounced at a height of $22m$ above the sea level, which coincides with the roof of the new hangar. The runway (18/36) remains unaffected.

Figure 8 of Appendix B shows the contours of wind speed and turbulence velocity at four different heights (22m, 18m, 14m and 10m) for the S-SE-erly wind direction. In this case the velocity deficit and wakes induced by the buildings can reach and intersect almost the middle of runway 18/36. This time the effect is most pronounced at a height of $18m$ above the sea level, which is close to the roof level of the old hangar, similar to the previous case. Runway 11/29 remains unaffected. Also it is clear that the existing hangar will shield the effect of the proposed building. However, in the absence of the old hanger the wakes induced by the new hangar buildings will be able to reach the runway.

Figure 9 and Figure 10 of Appendix B gives an idea about the turbulence on a vertical plane intersecting the runway 11/29 and the buildings.

In Figure 12 of Appendix B a direct comparison of turbulence velocities for N-NE-erly wind (25°) with free wind speeds of 20 m/s and 30 m/s is shown. The 20 m/s case is on the left side and the 30 m/s case on the right side of the figure. Results are given at elevations of 23, 33 and 43 m AMSL from top to bottom. It is evident that the 20 m/s free wind speed case does not create downwind zones of $U_t > 2.5$ m/s, except for the elevation

PROJECT
102011078

REPORT NUMBER
SINTEF A27618

VERSION
2.0

11 of 27

of 23 m AMSL (close to the elevation of the roof of the new hangar) just behind it. However, for *the storm case* (30 m/s free wind speed) this changes significantly. Parts of runway 11/29 are covered by zones with $U_t > 3$ m/s at all the elevations shown.

In Figure 13 of Appendix B a direct comparison of turbulence velocities for S-SE-erly wind (115°) with free wind speeds of 20 m/s and 30 m/s is shown. The 20 m/s case is on the left side and the 30 m/s case on the right side of the figure. Results are given at elevations of 13, 23 and 33 m AMSL from top to bottom. As for the N-NE wind case it is evident that the 20 m/s free wind speed case does not create downwind zones of $U_t > 2.5$ m/s. However, for *the storm case* (30 m/s free wind speed) this changes significantly. Parts of runway 18/36 are covered by zones with $U_t > 3$ m/s at all the elevations shown.

Figure 14 shows a comparison of turbulence velocities for the N-NE-erly and the S-SE-erly *storm case scenarios* by plotting turbulence velocities along vertical lines right above the runway crossing point with the hangar crossing wind direction line in both cases. Observe that the impact of the new hangar (red curve) is slightly less than that of the old hangar (green curve) on their respective (closest) runways when wind conditions are the same except for the wind direction.

5 Summary and Conclusions

The main goal of this analysis was to find out if a planned construction of a new helicopter hangar at Stavanger Airport Sola would cause unwanted impact on flight conditions over the runways and their nearby areas. Even though the old helicopter hangar will be removed in near future, it was decided to study the impact of that hangar as well, in particular for the potential of a combined, unwanted impact (strong wind shear and building induced turbulence) from the old and the new hangar while they both are standing there. Spatio-temporal variations of wind velocity can cause strong wind shear and turbulence resulting in a sudden gain or loss of altitude by the aircraft. This can pose a hazard especially during the landing and takeoff phase of flights. The wind shear can be caused due to the terrain (hills, mountains) or built structures (hangers, buildings, towers). Additionally, a vertical temperature gradient can also induce buoyancy induced turbulence. Since, the area under investigation is characterized by stable stratification which results in suppression of turbulence we have confined ourself to isothermal cases which are considered more severe. Turbulence intensity, in terms of which we normally present our results accounts for this wind shear. The quantity has been used in different kinds of studies like terrain induced turbulence in Rasheed and Sørli (2013), siting of runways in Rasheed et al. (2011), real-time forecasting in Rasheed and Sørli (2014) and more recently in building-induced turbulence modeling in Tabib and Rasheed (2015) and Rasheed et al. (2014).

In the current scenario worst condition is expected to be associated with three different wind directions so corresponding simulations were conducted, i.e. 25° (north-northeasterly (N-NE)), 115° (east-southeasterly (E-SE)) and 270° (westerly (W)) were simulated. The last wind direction (W) was added because this is the prevalent wind direction at the given site. However, it was not expected to give negative effects at all from the hangar buildings on the air traffic on any of the runways. The simulations that were conducted for this wind direction confirmed our assumption. The other two wind directions (N-NE and E-SE) were chosen in order to simulate presumptively the most severe conditions for the runways, caused by wind perpendicular to the new and the old hangar, respectively. This generates a *turbulent wake* between the hangar and the runway. The main question is whether or not this wake will extend all the way down to and possibly over the runway, and at the same time being so strong as to influence landing and departing aircraft. As mentioned above, we have investigated both how the wind changes as well as the turbulence over the runways with the given wind directions. The following conclusions were made after all the simulations were completed and the results were visualized (see selected plots in figures 7, 8) and analyzed:

1. Westerly winds (270°) (the prevalent winds at the site) create no problems caused by neither the old nor the new hangar when analysed in a separate manner, their wakes are located far away from the runways. However, it should be mentioned that the terminal buildings that are located on the upwind side of RWY 18/36 in this wind case scenario, are not part of the simulation setup. Our task in the present work was to

study the impact of the new and the old hangar separately and in mutual interaction.

2. North-northeasterly (N-NE, 25°) winds create flight conditions which are in the "borderline" when it comes to unwanted effects from the NEW hangar. This is a wind direction which, together with the new hanger are making the longest and strongest turbulent wakes in the direction of runway 29. The wind field may create a wind shear at this runway in this case. Turbulence is light to moderate over the runway for free stream wind speeds of $20m/s$ (*fresh gale*) at $1500m$ AMSL. Since it is assumed that the atmosphere is *neutral* for all the simulations, the results can be scaled linearly with increasing free stream wind speed. Measurements at Sola have at times shown wind speeds as large as $30m/s$ (*violent storm*) for the mean wind. This means that we can multiply the turbulence velocity by a factor of 1.5 in that case. Then we move from $U_t = 2$ to $U_t = 3$ over the runway, and we have moved from light/moderate turbulence to moderate/severe turbulence. The conclusion is therefore that the new hangar imply acceptable flight conditions (light to moderate turbulence) at runway 29 for a N-NE-erly wind direction and free stream wind speeds up to 20 m/s, while real stormy weather with free stream wind speeds of 30 m/s can give severe turbulence over runway 29 caused by the new hangar.

3. East-southeasterly (S-SE, 115°) winds create flight conditions which are in "borderline" when it comes to unwanted effects from the OLD hangar. This is a wind direction which, together with the old hangar are making the longest and strongest turbulent wake in the direction of RWY 18/36. The wind field may create a wind shear at this runway. Turbulence is light to moderate over the runway, but as for the previous scenario (N-NE-erly wind), the conditions change when the free stream wind speed is increased from 20 m/s to 30 m/s (from fresh gale to violent storm). The conditions actually become a bit worse here than for the case of the new hangar and N-NE-erly wind. The conclusion is therefore that the old hangar imply acceptable flight conditions (light to moderate turbulence) at runway 18/36 for S-SE-erly wind direction and free stream wind speeds up to 20 m/s, while real stormy weather with free stream wind speeds of 30 m/s can give severe turbulence caused by the old hangar.

4. We found no unfavorable combined effects from the new and the old hangar by performing the simulations and analyzing the results. There was a potential for combined effects for the E-SE-erly winds, but the simulations only indicate very minor effects in that direction. The conclusion is therefore that there will be no unfavorable flight conditions at RWY 18/36 as a result of a combined effect from old and new hangar in the period when both are present at the airport.

5. Another matter that needs to be mentioned is that the new and planned hangar is less unfavorable with respect to turbulent wakes than the old one when they are compared with their separate and most unfavorable wind directions N-NE and S-SE, respectively.

In other word, the new hangar can worsen flight conditions at runway 29, but its unfavorable impact will not be as large as the old hangar and its impact on flight conditions on RWY 18/36.

Acknowledgements

SINTEF

References

Clark, T., Keller, T., Coen, J., Neilley, P., Hsu, H.-M., and Hall, E. (1997). Terrain-induced Turbulence over Lantau Island: 7 june 1994 tropical storm russ case study. *Journal of Atmospheric Science*, 54:1795–1814.

Eidsvik, K., Holstad, A., and Utnes, T. (2004). A prediction system for local wind variation in mountainous terrain. *Boundary Layer Meteorology*, 112:557–586.

Huang, S., Li, Q., and Xu, S. (2007). Numerical evaluation of wind effects on a tall steel building by CFD. *J. Constructional Steel Research*, 63(5):612–627.

Krüs, H., Haanstra, J., van der Ham, R., and Wichers Schreur, B. (2003). Numerical simulations of wind measurements at Amsterdam Airport Schiphol. *Wind Engineering and Industrial Aerodynamics*, 91(10):1215–1223.

Neofytou, P., Venetsanos, A., Vlachogiannis, D., Bartzis, J., and Scaperdas, A. (2006). CFD simulations of the wind environment around an airport terminal building. *Environmental Modelling & Software*, 21(4):520–524.

Rasheed, A. and Sørli, K. (2013). CFD Analysis of Terrain Induced Turbulence at Kristiansand Airport Kjevik. *Aviation*, 17:104–112.

Rasheed, A. and Sørli, K. (2014). A multiscale turbulence prediction and alert system for airports in hilly regions. *IEEE Aerospace Conference*, ISBN:978-1-4799-5582-4:1–10.

Rasheed, A., Sørli, K., and Midtbø, K. (2011). Analysis and siting of a new runway at the Sandnessjøn Airport Stokka with respect to mountain induced turbulence. *SINTEF Report*, F20557.

Rasheed, A., Tabib, M., and Sørli, K. (2014). Investigation of flying conditions at the Stavanger Airport Sola using numerical simulations. *SINTEF Report*, F26399.

Senthooran, S., Lee, D., and Parameswaran, S. (2004). A computational model to calculate the flow-induced pressure fluctuations on buildings. *J. Wind Engineering and Industrial Aerodynamics*, 92(13):1131–1145.

Tabib, M. and Rasheed, A. (2015). Impact analysis of the proposed parking lot on the flying condition close to the Kristiansund Airport. *SINTEF Report*, F26978.

Appendices

A Plots of Model Setups

Figure 1: Image overlay of hangar buildings in *Google Earth*. UTM coordinates of the buildings are thereafter found. Notice that a certain level of *image transparency* is necessary to get a good enough match between the overlay image and the Google Earth image. Notice also that the centerlines of the runways are marked for the case of the subsequent analysis.
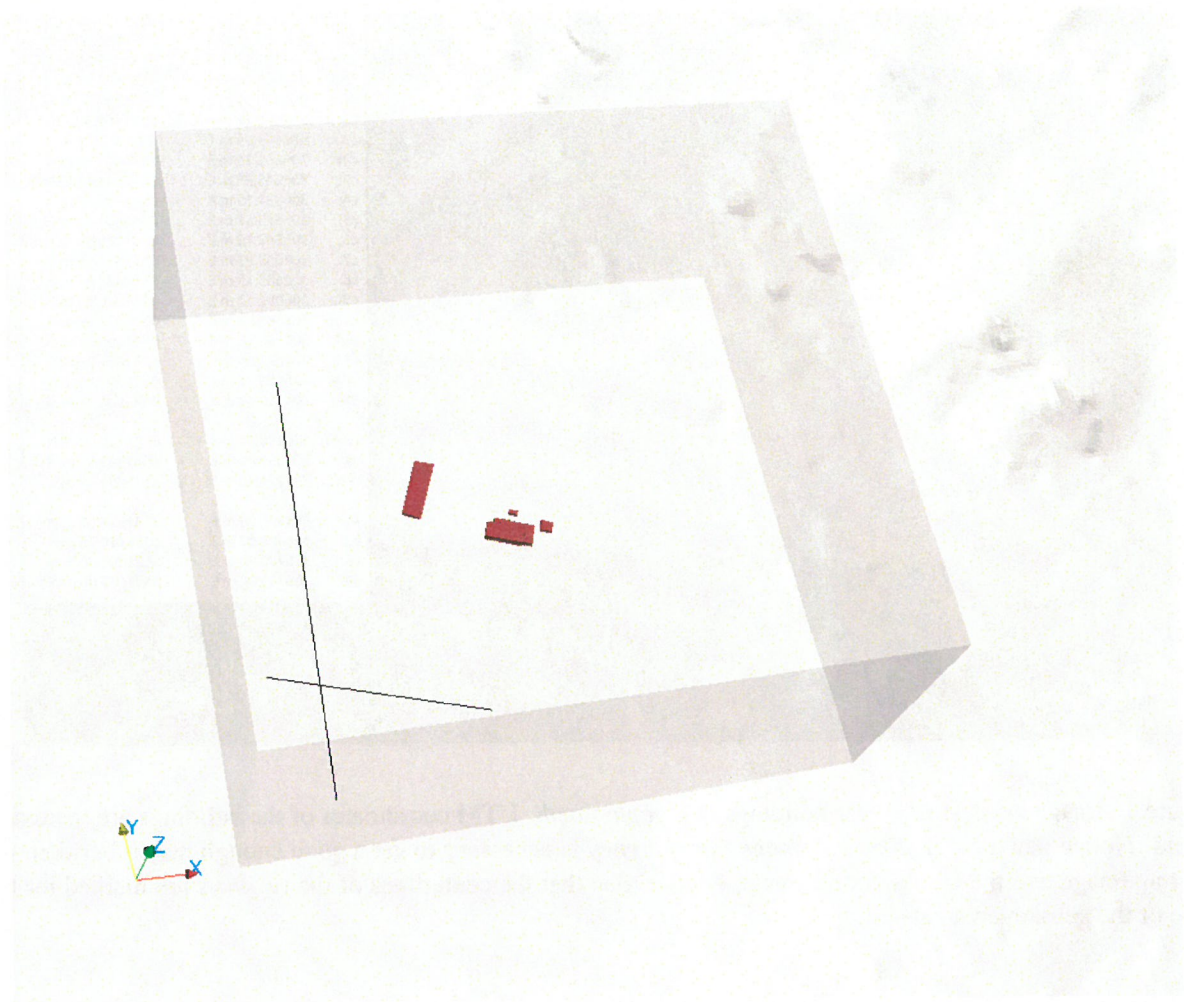
PROJECT
102011078

REPORT NUMBER
SINTEF A27048

VERSION
2.0

14 of 27

Figure 2: A 3D perspective plot of the computational domain ($750 \times 750 \times 500 \, m^3$) with hangar buildings and center lines of the runways.

PROJECT
102614078

REPORT NUMBER
SINTEF A27048

VERSION
2.0

15 of 27
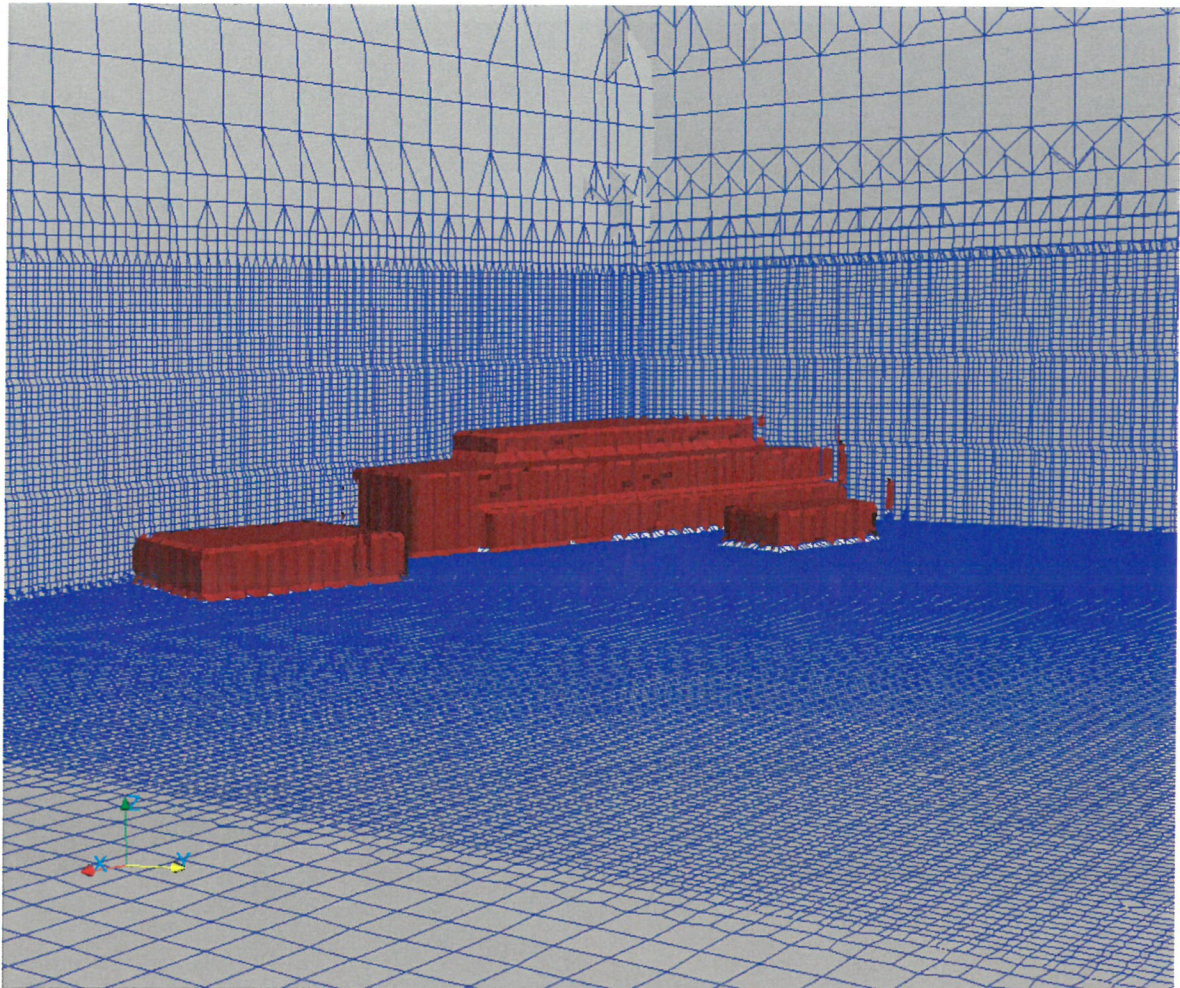
Figure 3: A 3D hybrid and adapted mesh was utilized with a strong refinement towards the buildings in order to resolve the fine physics that exist near the building corners, edges and surfaces.

PROJECT
102012078

REPORT NUMBER
SINTEF 627065

VERSION
2.0

16 of 27
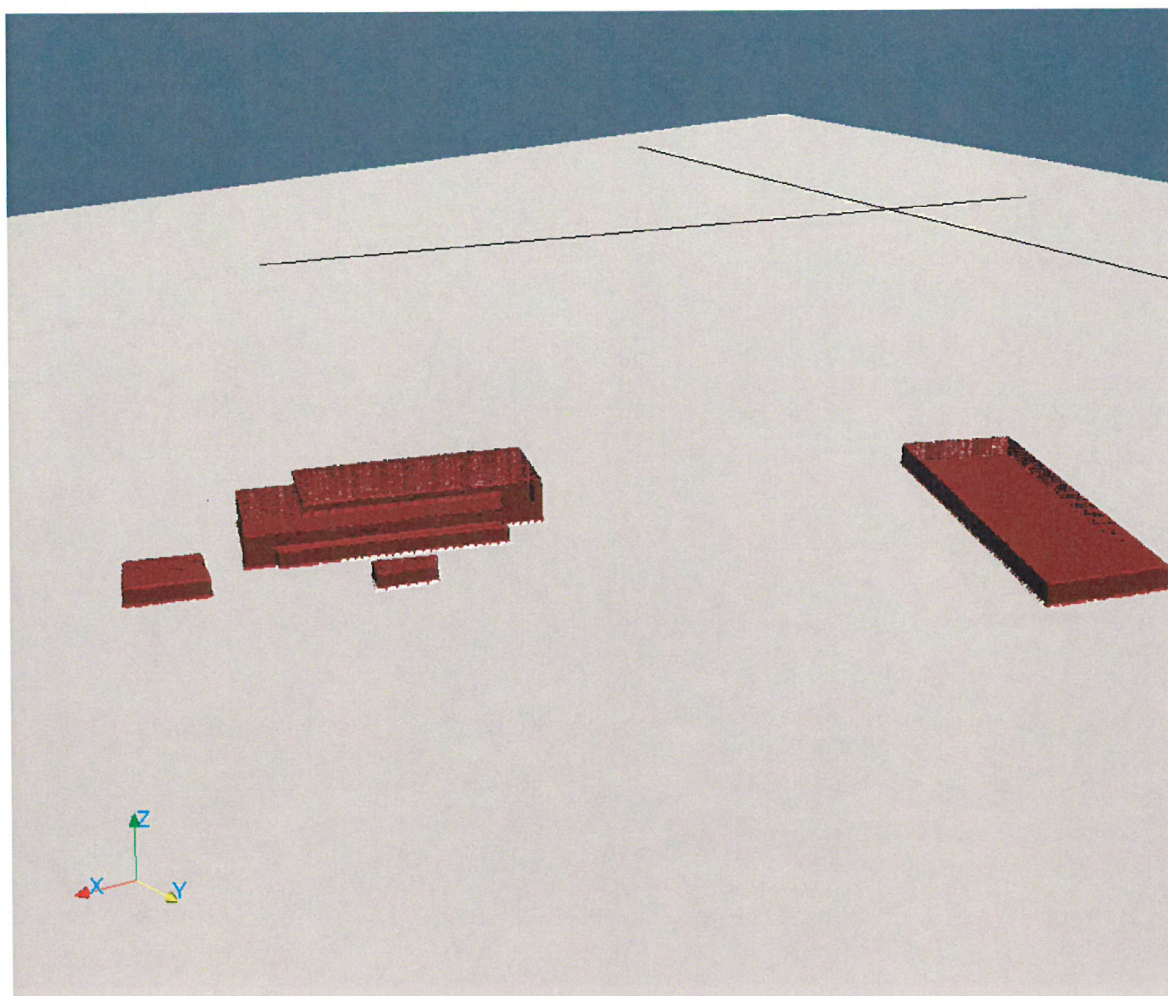
Figure 4: New (left) and old (right) hangar buildings with center lines of both runways at the Sola Airport.

PROJECT
102011078

REPORT NUMBER
SINTEF A27018

VERSION
2.0

17 of 27
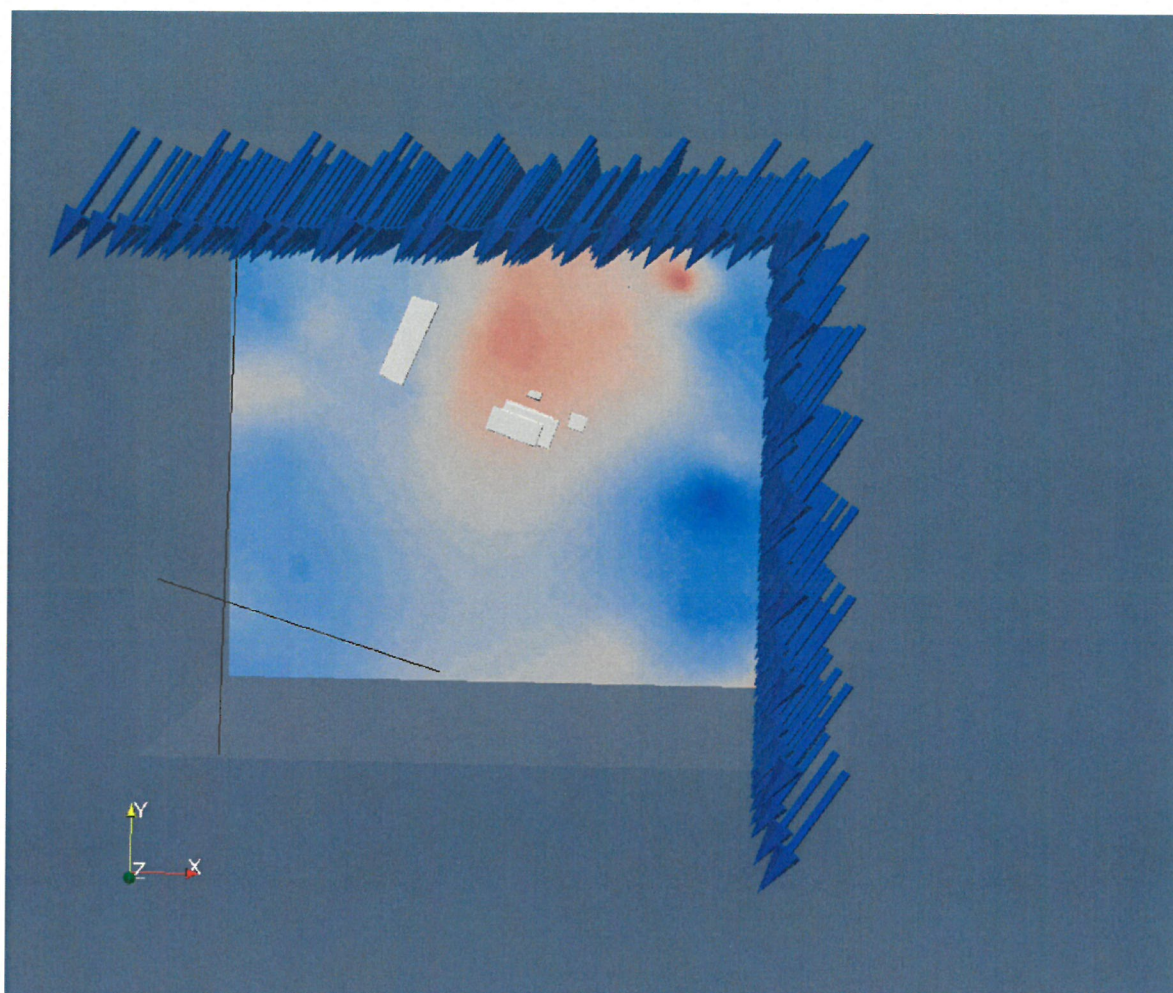
Figure 5: Illustration of wind conditions at boundaries for the N-NE-erly case. Small variations of the ground surface are rendered as well.
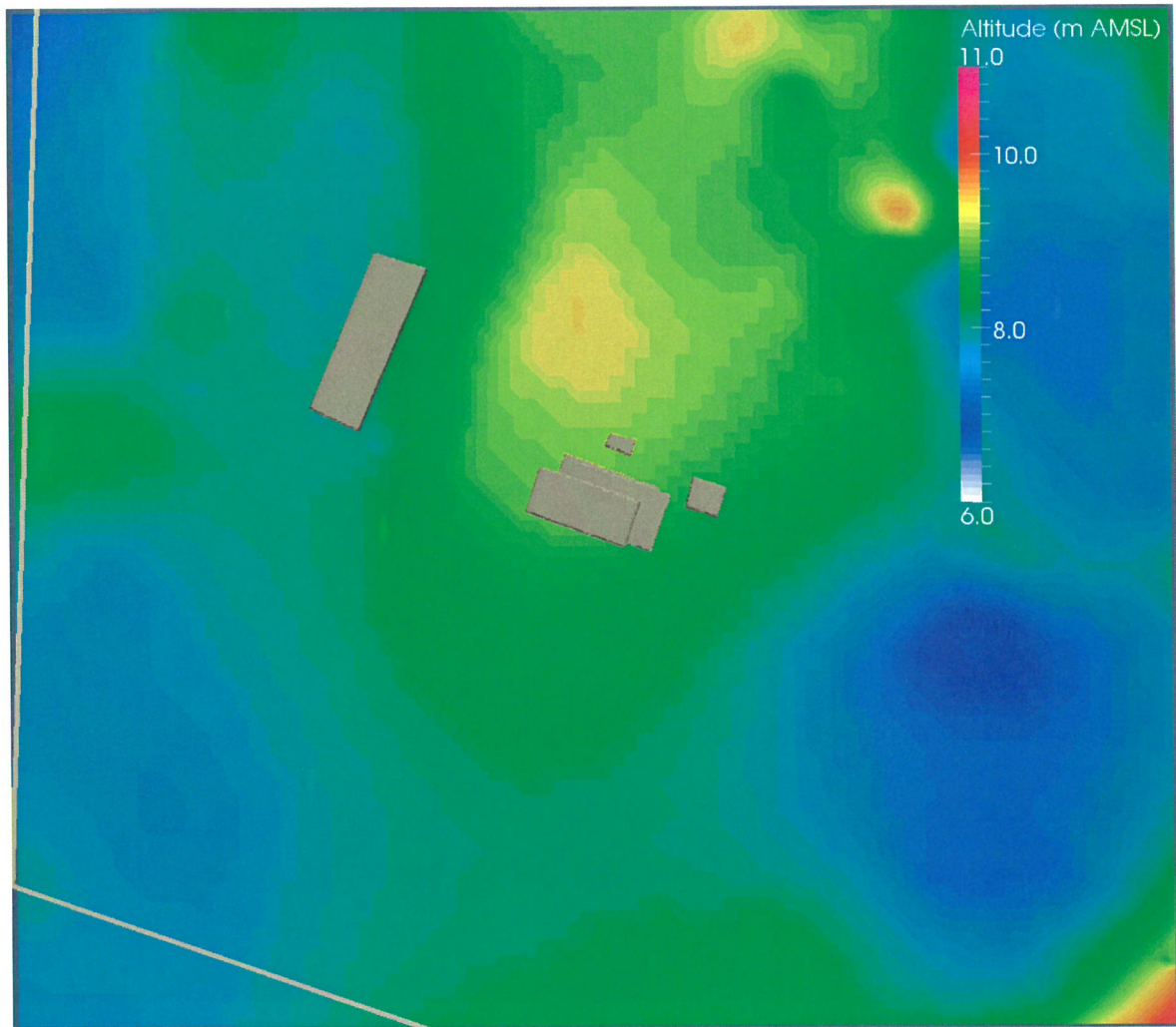
Figure 6: Terrain heights within the computational region.
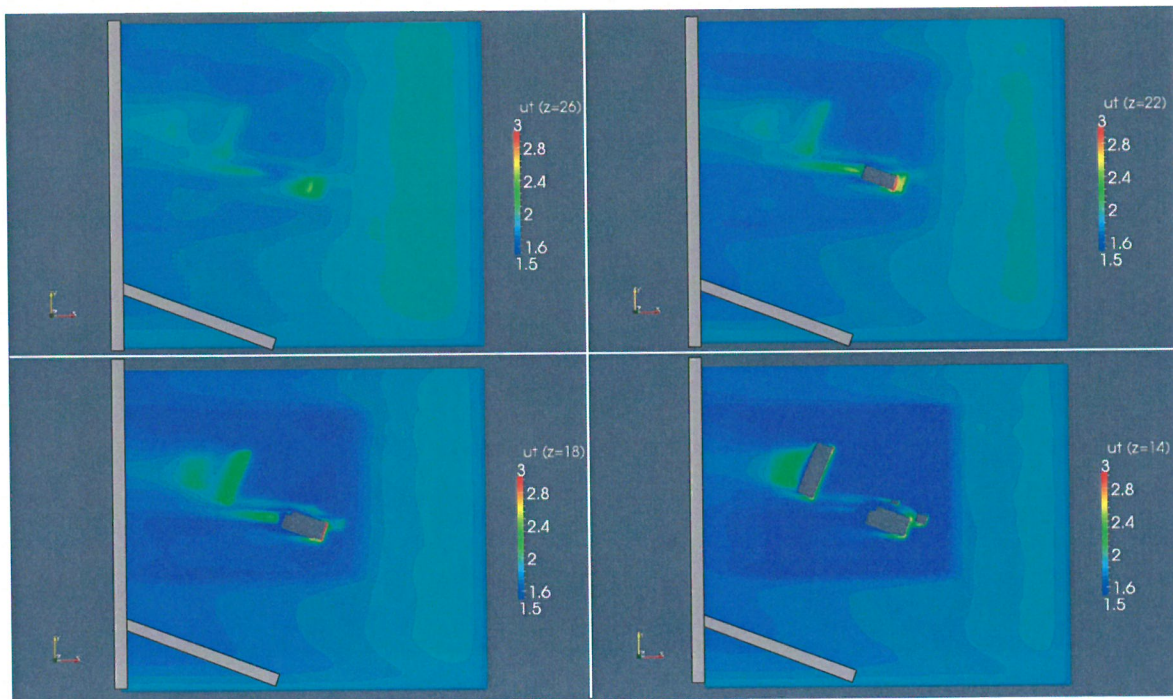
B Plots of Simulation Results
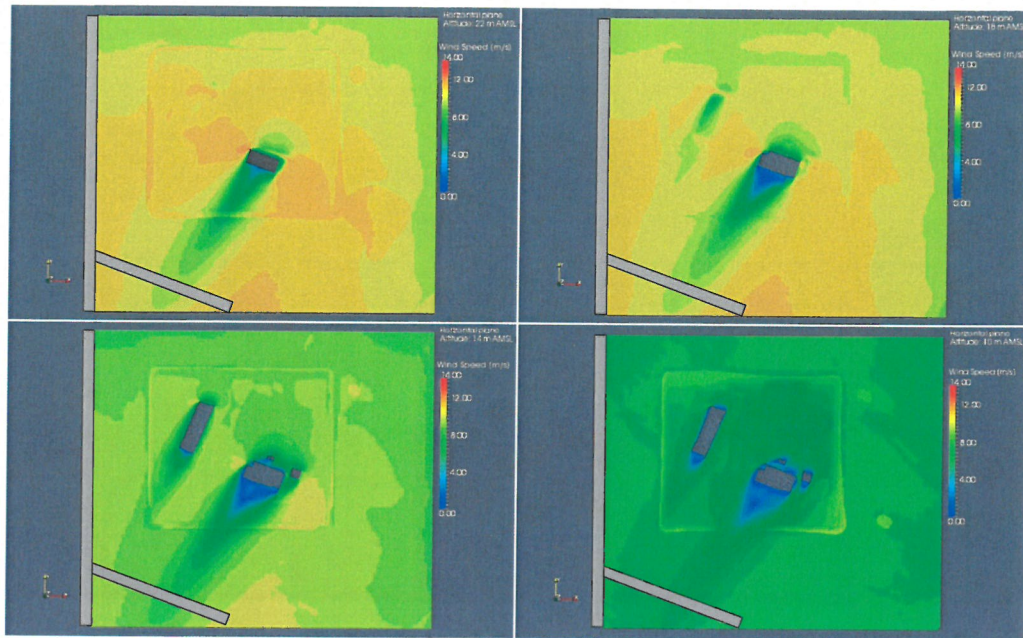
(a)
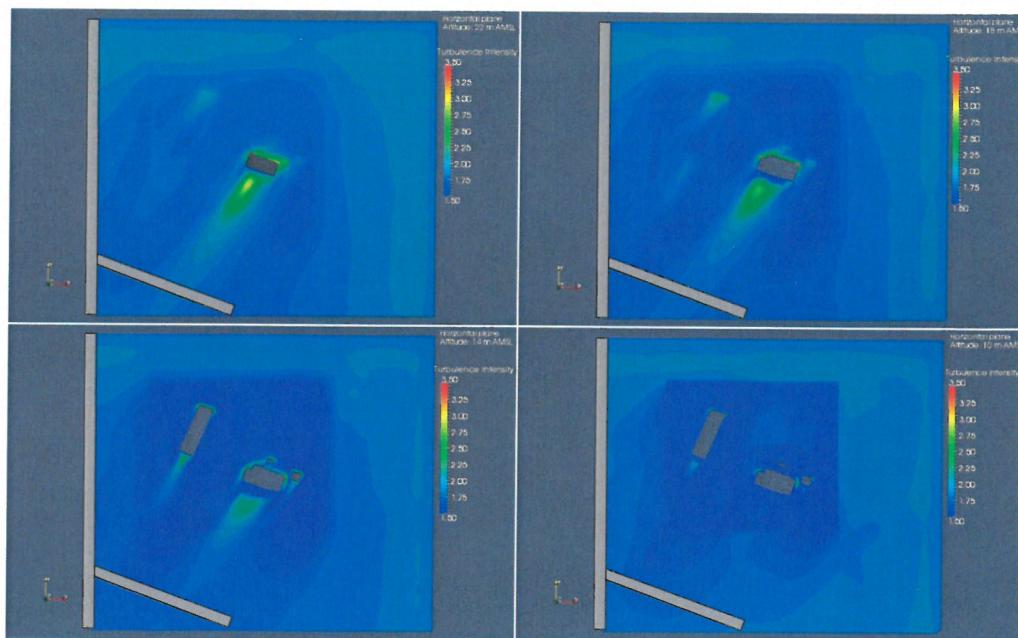
(b)

Figure 7: Simulation results for N-NE-erly wind direction (25°). (a) Plot of wind speed (U, m/s) and (b) Plot of turbulence velocity (U_t, m/s), in four different horizontal planes: 22m, 18m, 14m and 10m AMSL.
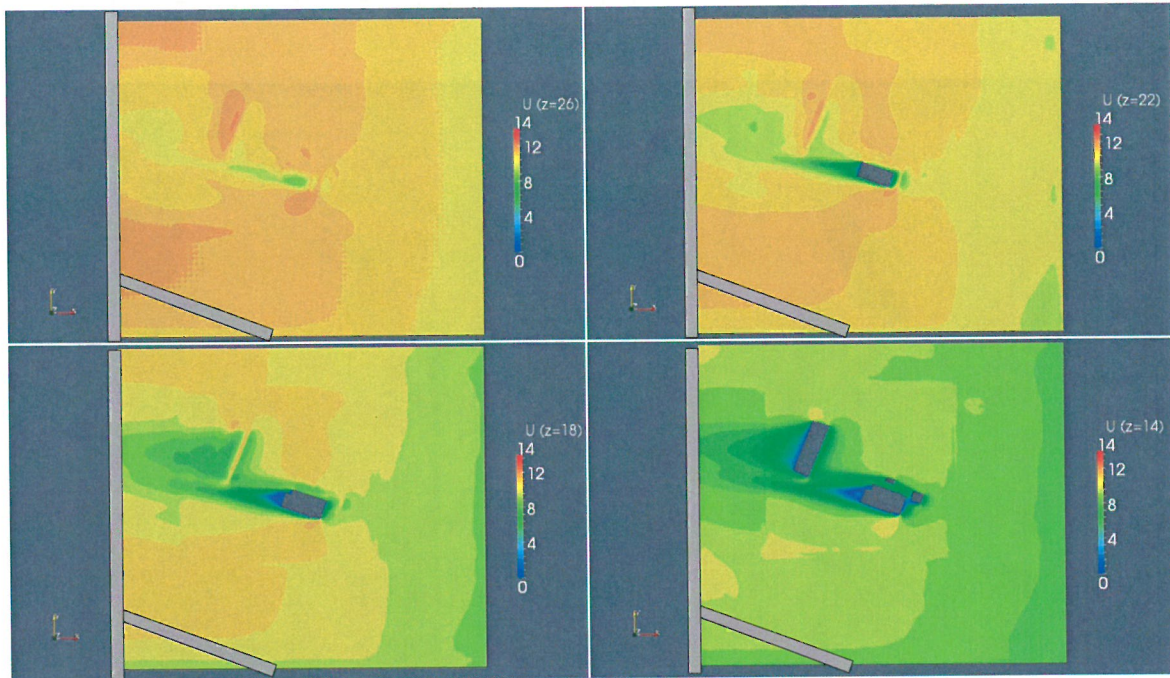
(a)

(b)

Figure 8: Simulation results for S-SE-erly wind direction (115°). (a) Plot of wind speed (U, m/s) and (b) Plot of turbulence velocity (U_t, m/s), in four different horizontal planes: 26m, 22m, 18m and 14m AMSL.

Figure 9: Simulation results for N-NE-erly wind direction (25°) and the free wind speed of 20 m/s. Plot of turbulence velocity in vertical plane through new hangar.
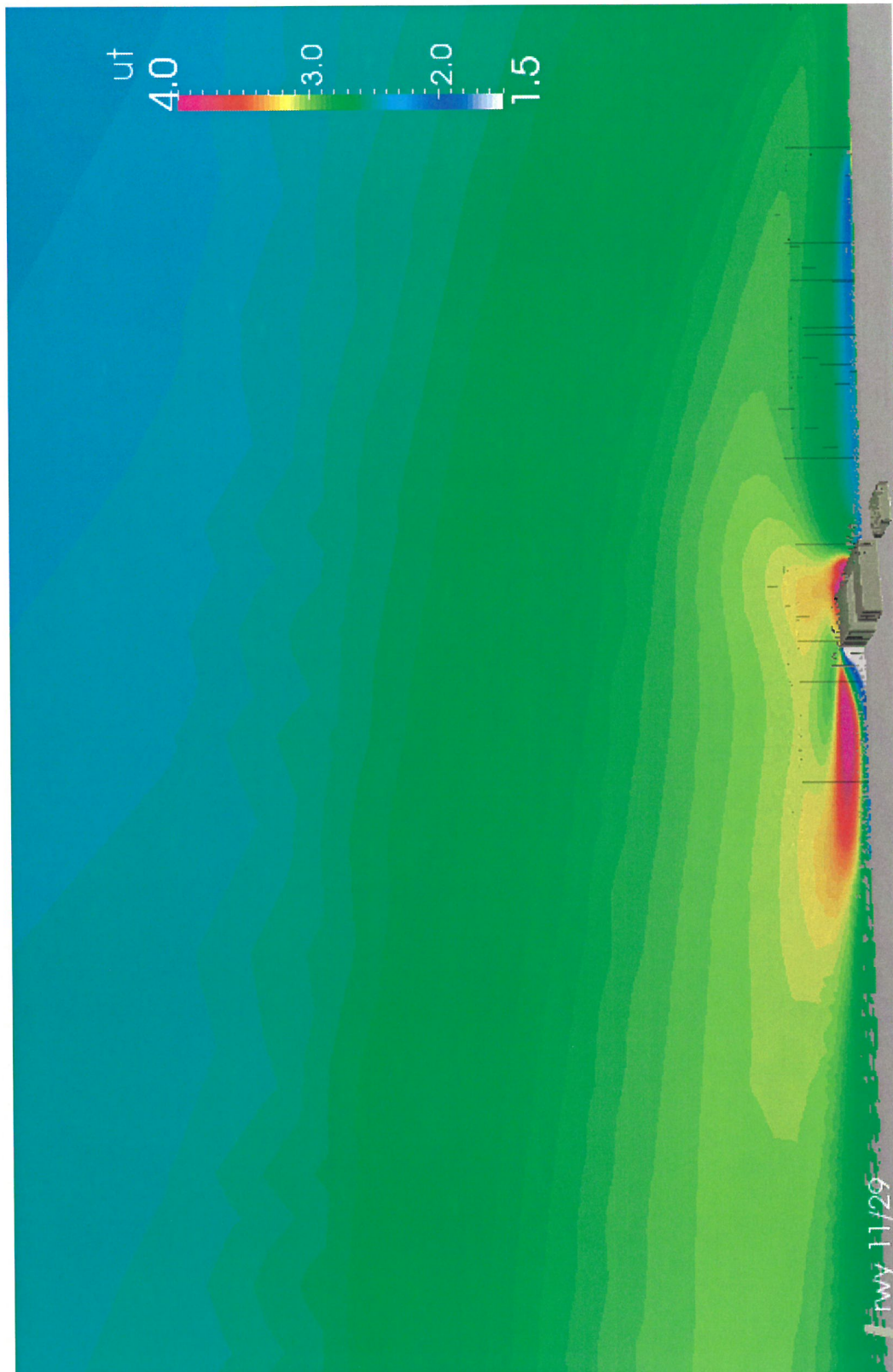
PROJECT
102011078

REPORT NUMBER
SINTEF A27055

VERSION
2.0

22 of 27

Figure 10: Simulation results for N-NE-erly wind direction (25°) and the free wind speed of 30 m/s. Plot of turbulence velocity in vertical plane through new hangar.

PROJECT
102011028

REPORT NUMBER
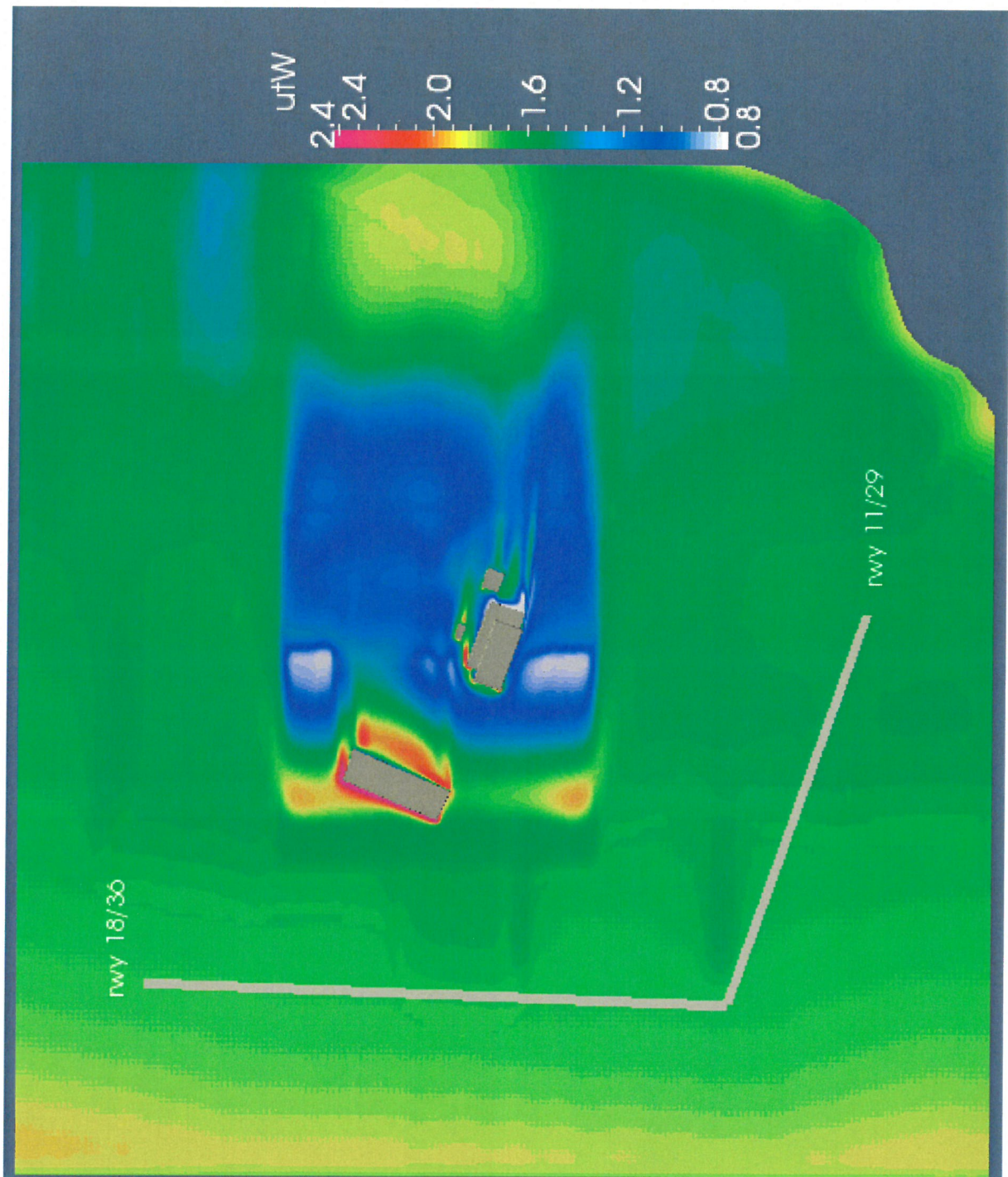SINTEF A23948

VERSION
2.0

24 of 27

Figure 11: Simulation results for W-erly wind direction (270°) and the free wind speed of 20 m/s. Plot of turbulence velocity in horizontal plane at height 14m AMSL.

PROJECT
102G1107A

REPORT NUMBER
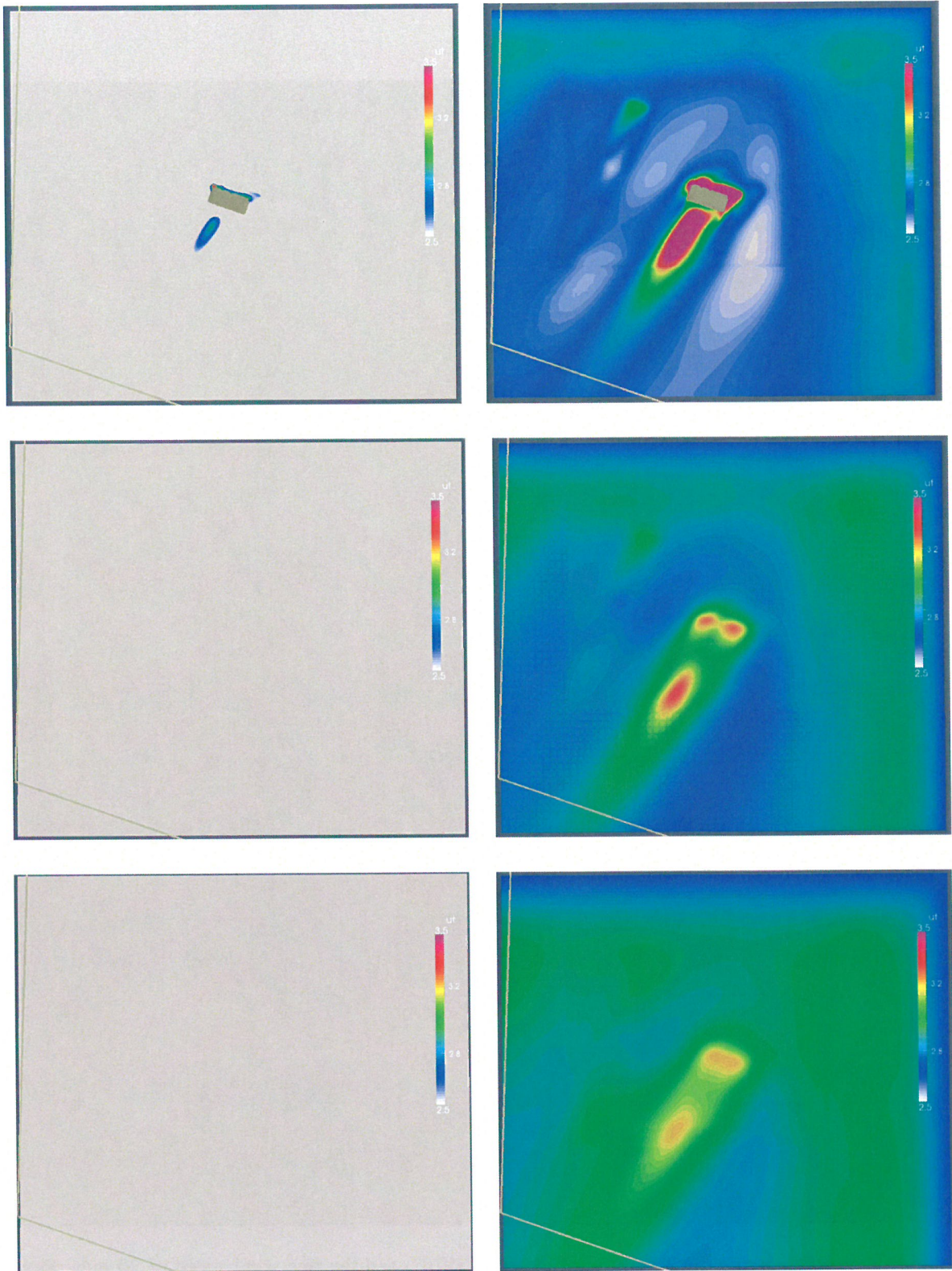SINTEF A23648

VERSION
2.0

24 of 27

Figure 12: Comparison of turbulence velocities for N-NE-erly wind direction (25°) with free wind speeds of 20 m/s and 30 m/s. The 20 m/s case on the left side and the 30 m/s case on the right side. Elevations of 23, 33 and 43 m AMSL from top to bottom.
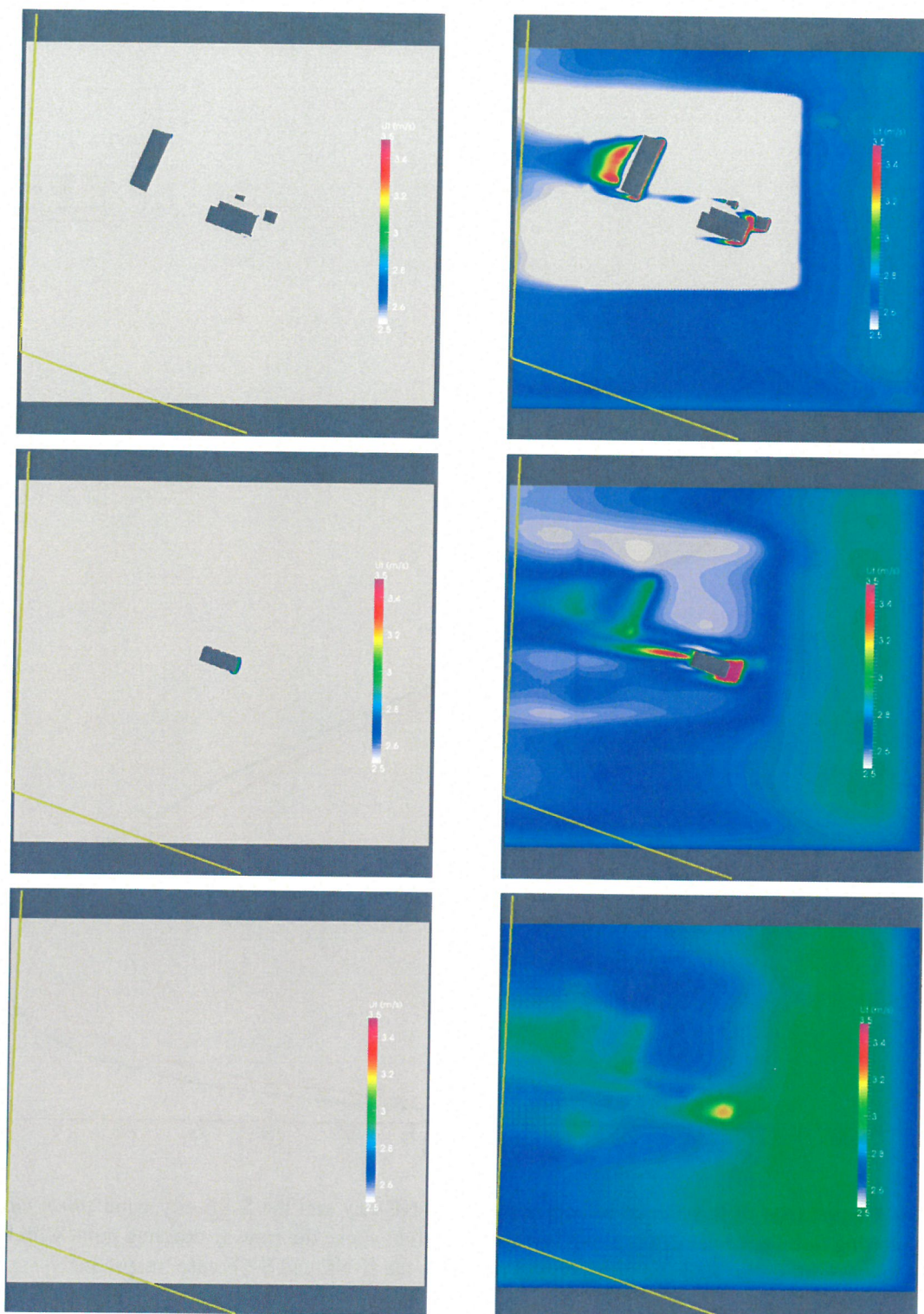
Figure 13: Comparison of turbulence velocities for S-SE-erly wind direction (115°) with free wind speeds of 20 m/s and 30 m/s. The 20 m/s case on the left side and the 30 m/s case on the right side. Elevations of 13, 23 and 33 m AMSL from top to bottom.
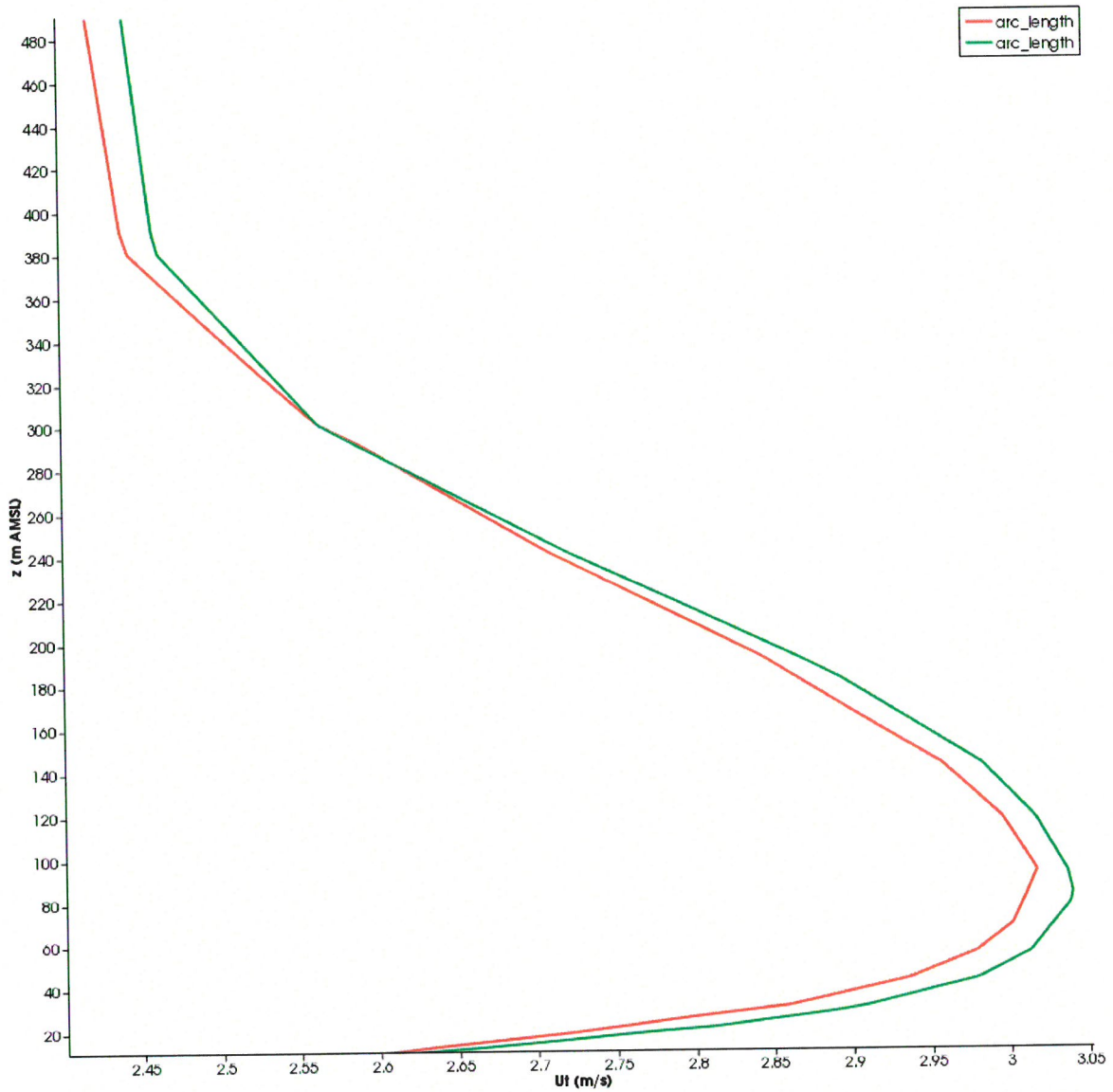
Figure 14: Comparison of turbulence velocities for the N-NE-erly and the S-SE-erly wind *storm case scenarios* by plotting turbulence velocities along vertical lines right above the runway crossing point with the wind direction line in both cases. Red and green curves represent the N-NE and S-SE case, respectively.

PROJECT
102011078

REPORT NUMBER
SINTEF 2017045

VERSION
2.0

27 of 27